

Article

Facile Synthesis of ZnSe/Co₃O₄ Heterostructure Nanocomposites for the Photocatalytic Degradation of Congo Red Dye

Adeel Zia ^{1,2} , Abdul Basit Naveed ¹, Aftab Javaid ¹, Muhammad Fahad Ehsan ^{1,3,*} and Azhar Mahmood ^{1,*} 

¹ Department of Chemistry, School of Natural Sciences, National University of Sciences and Technology, Islamabad 44000, Pakistan

² School of Chemistry and Chemical Engineering, Shanghai Jiao Tong University, Dongchuan Road, District Minhang, Shanghai 200240, China

³ Verschuren Center for Sustainability in Energy and Environment, Cape Breton University, Sydney, NS B1P 6L2, Canada

* Correspondence: m.fahad.ehsan@sns.nust.edu.pk (M.F.E.); dr.azhar@sns.nust.edu.pk (A.M.); Tel.: +92-51-90855574 (A.M.)

Abstract: In the present paper, simple hydrothermal and solid-state methods are reported for the synthesis of metal chalcogenide (ZnSe), metal oxide (Co₃O₄) and their nano-heterostructure (ZnSe/Co₃O₄ 3:1, 1:1 and 1:3 ratios by weight), while their photocatalytic efficiencies are also investigated. The X-ray diffraction results corroborate the good crystallinity and purity of all synthesized products, i.e., ZnSe, Co₃O₄ and their nanocomposites. The scanning electron micro-images of ZnSe show a mixed morphology of nanoparticles (≈ 16 nm), including spherical and distorted cubes, while Co₃O₄ has a worm-like morphology ($\approx 20 \times 50$ nm). The EDX results show that all the elements are present in accordance with their anticipated amounts in the products. The UV/visible absorption spectrum of ZnSe depicts a sharp absorption at around 480 nm, while Co₃O₄ demonstrates two prominent peaks, 510 nm and 684 nm. The prepared samples were employed for the photocatalytic degradation of Congo red dye and the nano-heterostructure (ZnSe/Co₃O₄ 3:1) shows an exceptional photocatalytic degradation efficiency of 96%. This enhanced photocatalytic activity was due to the synergic effect of ZnSe and Co₃O₄ that reduced the electron/hole recombination and caused suitable bandgap alignment.

Keywords: nanomaterials; photocatalysis; ZnSe; Co₃O₄; heterostructure; Congo red



Citation: Zia, A.; Naveed, A.B.; Javaid, A.; Ehsan, M.F.; Mahmood, A. Facile Synthesis of ZnSe/Co₃O₄ Heterostructure Nanocomposites for the Photocatalytic Degradation of Congo Red Dye. *Catalysts* **2022**, *12*, 1184. <https://doi.org/10.3390/catal12101184>

Academic Editor: Ewa Kowalska

Received: 12 December 2021

Accepted: 26 January 2022

Published: 7 October 2022

Publisher's Note: MDPI stays neutral with regard to jurisdictional claims in published maps and institutional affiliations.



Copyright: © 2022 by the authors. Licensee MDPI, Basel, Switzerland. This article is an open access article distributed under the terms and conditions of the Creative Commons Attribution (CC BY) license (<https://creativecommons.org/licenses/by/4.0/>).

1. Introduction

The modern world is suffering from severe environmental pollution due to the unchecked release of various toxic materials. Toxic gases, e.g., chlorofluorocarbons, carbon monoxide and carbon dioxide, are causing air pollution, while toxic chemicals, e.g., azo dyes, are causing water pollution. The azo dyes, similar to methyl orange, Congo red and methylene blue, released by the textile and leather industries are causing severe water pollution [1]. The azo dyes are the most stable type of organic pollutants and they further convert into stable hazardous products [2]. Hence, the removal of these dyes from the water by converting them into non-toxic by-products is crucial.

Various strategies have been employed and various are under way to overcome water pollution. Among the different techniques, photocatalytic dye degradation is the most effective due to its environmentally friendly, reusable and cost-effective nature [3]. The other techniques, such as membrane filtration [4,5], electro-catalysis [6,7], precipitation [8], adsorption [9] and biological treatment [10], are expensive and require advanced setups, but photocatalytic degradation needs an effective catalyst and sunlight. Many researchers have reported various photocatalysts with an excellent dye degradation efficiency. The different

metal oxides, e.g., Co_3O_4 [11], ZnO [12,13], TiO_2 [14,15]; metal chalcogenides, e.g., ZnSe [16], ZnTe [17]; metal sulfides, e.g., CuS [18], CdS [19], ZnS [20,21] and their nanocomposites [22,23], are extensively employed as photocatalysts owing to their ease of synthesis, low cost and excellent photocatalytic properties. All the aforementioned semiconductor materials have a suitable bandgap for the acceleration of electrons from conduction band to valence band, under solar energy. The produced electron-hole pairs are the key for redox reactions that convert harmful organic dyes into harmless substances [24]. However, the efficiency of a single semiconductor photocatalysts possesses some limitations, such as a low solar energy response and fast electron-hole recombination. To overcome these limitations, several effective techniques are proposed, including (i) metal doping by different metals, e.g., Al, Cu, Ni, Co [25]; (ii) nano-structuralization by controlling the morphology of synthesized products, e.g., nanorods [26], nanowires and nanoplates [27]; and (iii) the development of heterostructure, e.g., SnO_2/GO [28], $\text{Co}_3\text{O}_4/\text{CoTe}$ [29], CuO/ZnO [30], ZnTe/ZnSe [31] and CNT/TiO_2 [32]. These techniques can lead the solar energy response to UV/visible and visible regions. Moreover, they reduce the electron-hole recombination. The development of heterostructure is a well examined and highly reported technique due to the much improved efficiency of heterostructures. In this technique, two photocatalysts can be combined in the form of a single nanocomposite to benefit from the photocatalytic activity of both, simultaneously reducing the recombination of charge carriers.

In the present work, the strategy of developing a semiconductor heterostructure is explored. A cost-effective, simple hydrothermal method was employed, which also provides greater control over the reaction conditions, such as time and temperature. ZnSe and Co_3O_4 nanoparticles were synthesized, which are already reported as excellent candidates for the photocatalytic break down of organic pollutants. However, for the development of the $\text{ZnSe}/\text{Co}_3\text{O}_4$ nano-heterostructure, simple solid state extensive grinding was employed.

The aim of this study is to develop an excellent semiconductor photocatalyst with an increased solar energy response. To the best of our knowledge, the preparation of the $\text{ZnSe}/\text{Co}_3\text{O}_4$ heterostructure photocatalyst by solid state grinding has not been reported, to date. Therefore, the findings of the present work might be helpful for the development of new excellent photocatalysts for the treatment of environmental pollution.

2. Materials and Methods

2.1. Chemicals

Zinc powder (Zn, Sigma Aldrich, St. Louis, MA, USA, 99%), selenium powder (Se, Merck, Kenilworth, NJ, USA, 99%); cobalt chloride hexahydrate ($\text{CoCl}_2 \cdot 6\text{H}_2\text{O}$, Sigma Aldrich, St. Louis, MA, USA, 99%); potassium hydroxide (KOH, Sigma Aldrich, St. Louis, MA, USA, $\geq 85\%$); ethanol ($\text{C}_2\text{H}_5\text{OH}$, Sigma Aldrich, St. Louis, MA, USA, $\geq 99.5\%$) and urea ($\text{CH}_4\text{N}_2\text{O}$, Merck, Kenilworth, NJ, USA, $\geq 99.5\%$) are used for the synthesis of ZnSe and Co_3O_4 . All the chemicals are of an analytical grade and no further purification was performed. Table 1 shows the details of the conditions and chemicals employed for the synthesis.

Table 1. Conditions and chemicals used for the preparation of ZnSe and Co_3O_4 nanoparticles.

Sample Name	Temperature	Time	Chemical Used
ZnSe	120 °C	2 h	Zn powder, Se powder and KOH
Co_3O_4	120 °C	20 h	$\text{CoCl}_2 \cdot 6\text{H}_2\text{O}$ and $\text{CH}_4\text{N}_2\text{O}$

2.2. Synthesis of ZnSe

In a typical hydrothermal approach, a 30 mL solution of 3 molar KOH was prepared and then 0.65 g of Zn and 0.39 g of Se were added to it. After stirring for 1 h, the homogeneous solution was transferred to a Teflon-lined autoclave with a total capacity of 40 mL. The closely tight autoclave was placed in an oven at 120 °C and after 2 h it was cooled down naturally. The final product was obtained after centrifugation, washing and vacuum drying at 70 °C for 12 h.

2.3. Synthesis of Co_3O_4

The hydrothermal approach was also employed for the synthesis of Co_3O_4 . In the typical procedure, a beaker containing 30 mL of distilled water, 0.36 g of $\text{CoCl}_2 \cdot 6\text{H}_2\text{O}$ and 0.72 g of urea was stirred for 1 h to obtain a transparent homogeneous solution. Then, the solution was transferred into a Teflon-lined autoclave with a capacity of 40 mL and placed in an oven for 20 h at 120 °C temperature. After cooling naturally, the obtained sample was washed by deionized water and ethanol, and then dried overnight in a vacuum oven. The final product was obtained after annealing the sample in a furnace for 2 h at 300 °C, and the heating rate was set to the 2 °C/min.

2.4. Preparation of the $\text{ZnSe}/\text{Co}_3\text{O}_4$ Heterostructure

The nanocomposites were made by a simple solid state method in which a controlled amount of already synthesized ZnSe and Co_3O_4 were subjected into an agate mortar and pestle. The ZnSe and Co_3O_4 nanopowder was ground well for an adequate amount of time to obtain 3 nanocomposites with varying amounts of ZnSe and Co_3O_4 : 3:1, 1:1 and 1:3 named as Z1, Z2 and Z3, respectively, and the details are presented in Table 2.

Table 2. Nanocomposites with the weight% ratios of ZnSe and Co_3O_4 .

Sr. #	Composite Name	% of ZnSe by Weight	% of Co_3O_4 by Weight
1	Z1	75	25
2	Z2	50	50
3	Z3	25	75

2.5. Characterization

To study the crystal structure and phase analysis, a Bruker D8 focus X-ray diffractometer (XRD, Bruker, Billerica, MA, USA) with a Ni filter and $\text{Cu-K}\alpha$ radiation was used. The recorded angle 2θ ranged from 20° to 80° with a scan rate of 0.1°/min. For the investigation of morphology and elemental composition, a Hitachi S4800 scanning electron microscope (SEM, Hitachi, Tokyo, Japan) coupled with an energy dispersive X-ray (EDX) spectroscopy was employed. For the measurement of the optical bandgap energies, a Lambda 750 UV/Visible/NIR spectrophotometer (PerkinElmer, Waltham, MA, USA) was used. To study the bandgap alignment, the UV/visible diffuse reflectance spectra (DRS) was determined.

2.6. Photocatalytic Studies

To investigate the photocatalytic activity of the synthesized products, the photocatalytic degradation of the Congo red (CR) dye was performed under the UV/visible light. Congo red is a carcinogenic, chemically and thermally stable anionic diazo dye with a high environmental risk as an industrial effluent. During the photocatalytic experiment, 10 mg of each photocatalyst (ZnSe , Co_3O_4 and $\text{ZnSe}/\text{Co}_3\text{O}_4$) was dispersed in 80 mL of CR solution (100 mg/L), separately. Then, the reaction vessel was stirred in the dark for 20 min to establish the absorption/desorption equilibrium. A light source in the form of a 300 W Xenon arc lamp was placed 15 cm above the reaction vessel. Before the start of the photocatalysis, two control experiments were also performed: (i) first, a control experiment was performed without light, and (ii) second, a control experiment was performed without the catalysts. No catalytic activity was observed in both of the controlled experiments. In the next experiment, the photocatalytic activity was investigated under the illumination of UV/visible light. To measure the degradation efficiency, 5 mL from the irradiated suspension was taken out of the reaction vessel at a regular time interval of 5 min, followed by centrifugation and UV/visible spectroscopic analysis.

3. Results

3.1. Phase Analysis

The XRD analysis was performed to investigate the phase and purity of the synthesized products, as represented in Figure 1. The XRD results of the ZnSe, Co_3O_4 and ZnSe/ Co_3O_4 heterostructures indicated that the products with good crystallinity and purity were obtained. The XRD pattern of ZnSe indicated the presence of both cubic and hexagonal structures. The peaks of cubic ZnSe appeared at 27.2° , 45.1° , 53.5° , 65.9° and 72.7° (JCPDS 3-065-9602), while the peaks of hexagonal ZnSe were observed at 26.2° , 29.5° , 36.1° and 68.2° (JCPDS 1-080-008) [33]. The peaks of Co_3O_4 were in good agreement with the reported literature and confirmed the formation of a cubic structure (JCPDS: 42-1467) [34]. The XRD patterns of Z1 (75:25), Z2 (50:50) and Z3 (25:75) also confirmed that the ZnSe/ Co_3O_4 nanocomposites were successfully synthesized. In all of the nanocomposites, the peaks of both ZnSe and Co_3O_4 were present and when the amount of ZnSe gradually decreased, the peak intensity of ZnSe also decreased. On the other hand, when the amount of Co_3O_4 increased, the peak intensity also increased, which confirms that the nanocomposites with desired ratios were prepared successfully, as can be seen from samples Z1 to Z3.

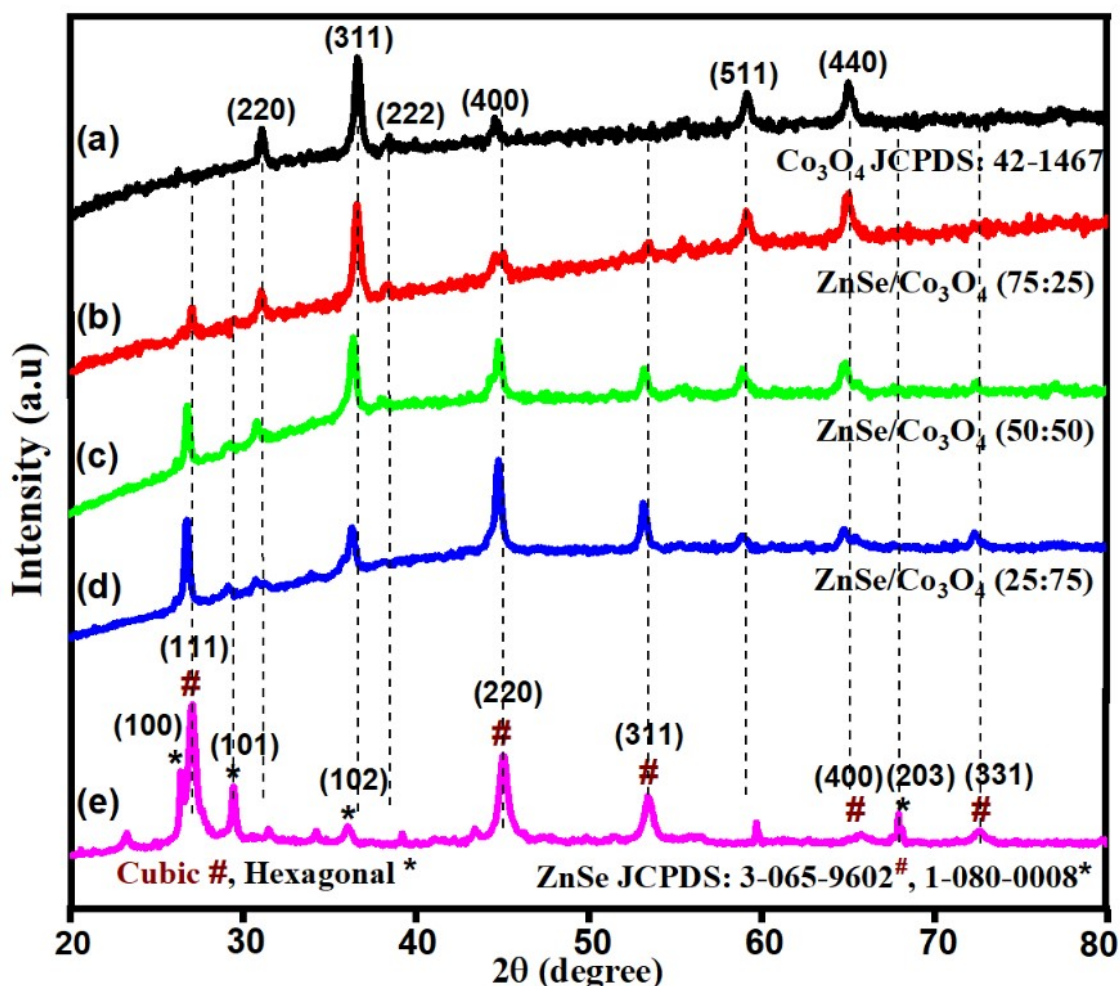


Figure 1. XRD results of (a) Co_3O_4 , (b) Z1, (c) Z2, (d) Z3 and (e) ZnSe. Cubic #, Hexagonal *.

3.2. Morphological Analysis

ZnSe shows a mixed morphology and is present in the form of agglomerates, as shown in Figure 2a. Most of the observed nanoparticles are spherical, while the others appeared as distorted cubes or grains, as observable in Figure 2a. The calculated size of the ZnSe nanoparticles is 16 nm, approximately, while Co_3O_4 shows worm-like congregates,

as represented in Figure 2b, with an approximate length of 50 nm and an approximate diameter of 20 nm. The particle size of both ZnSe and Co₃O₄ matches well with the size calculated by the Scherrer formula (ZnSe = 16.56 and Co₃O₄ = 20.32) represented by Equation (1).

$$C_s = \frac{0.94 \lambda}{\beta \cdot \cos \theta} \quad (1)$$

where C_s represents the crystallite size, 0.94 is the selected value for the Scherrer shape constant (K), assuming the crystallites to be spherical, λ is the wavelength of the incident X-rays, β is the full width-at-half maxima (fwhm) of a diffraction peak and θ is the Bragg's diffraction angle.

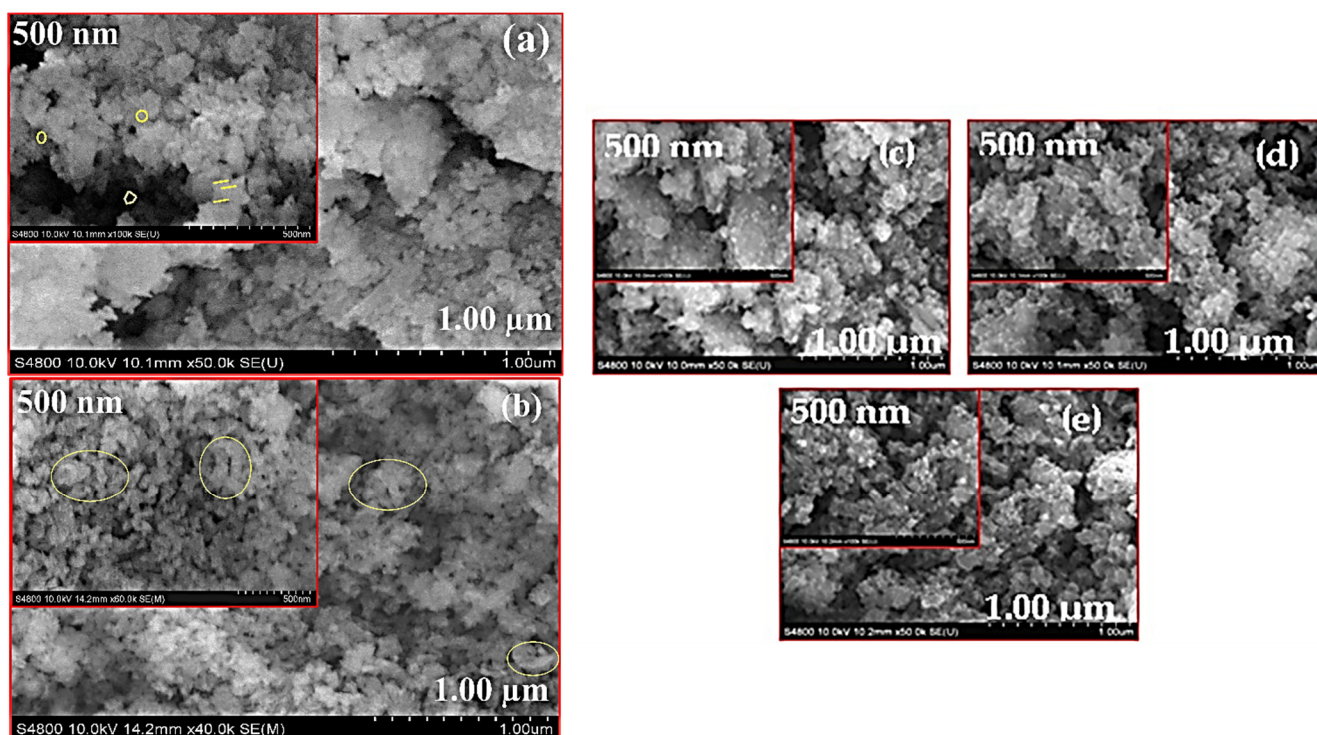


Figure 2. SEM images of (a) ZnSe, (b) Co₃O₄, (c) Z1, (d) Z2 and (e) Z3.

The nanocomposite Z1 contains a high amount of ZnSe compared to Co₃O₄. The SEM image (Figure 2c) of Z1 shows a high amount of grain-like structures and distorted cubes, while a low amount of worm-like morphologies were perceived, which confirms that a nanocomposite with 3:1 was successfully synthesized. The second nanocomposite named Z2 contained equal amounts of ZnSe and Co₃O₄, i.e., 1:1 by weight. The worm-like Co₃O₄ aggregates can be observed in the SEM image and the nanoparticles with a mixed morphology indicate the presence of ZnSe, as shown in Figure 2d. Nanocomposite Z3 (1:3) also contains both of the counterparts, ZnSe and Co₃O₄, but the amount of worm-like elongated nano-agglomerates is higher, which is an indicator of the enhanced proportion of Co₃O₄, as shown in Figure 2e. In general, these micrographs confirm the successful fabrication of nano-sized materials.

3.3. Elemental Analysis

To measure the elemental composition of ZnSe, Co₃O₄ and their heterostructure, an energy dispersive X-ray spectroscopy (EDX) was carried out. Figure 3a shows the EDX results of ZnSe with a high weight and atomic ratio of Zn and Se, which indicates the successful synthesis of the sample. Figure 3b shows the EDX analysis of Co₃O₄, which confirms the presence of both Co and O, while C is also present in a minute amount as an impurity.

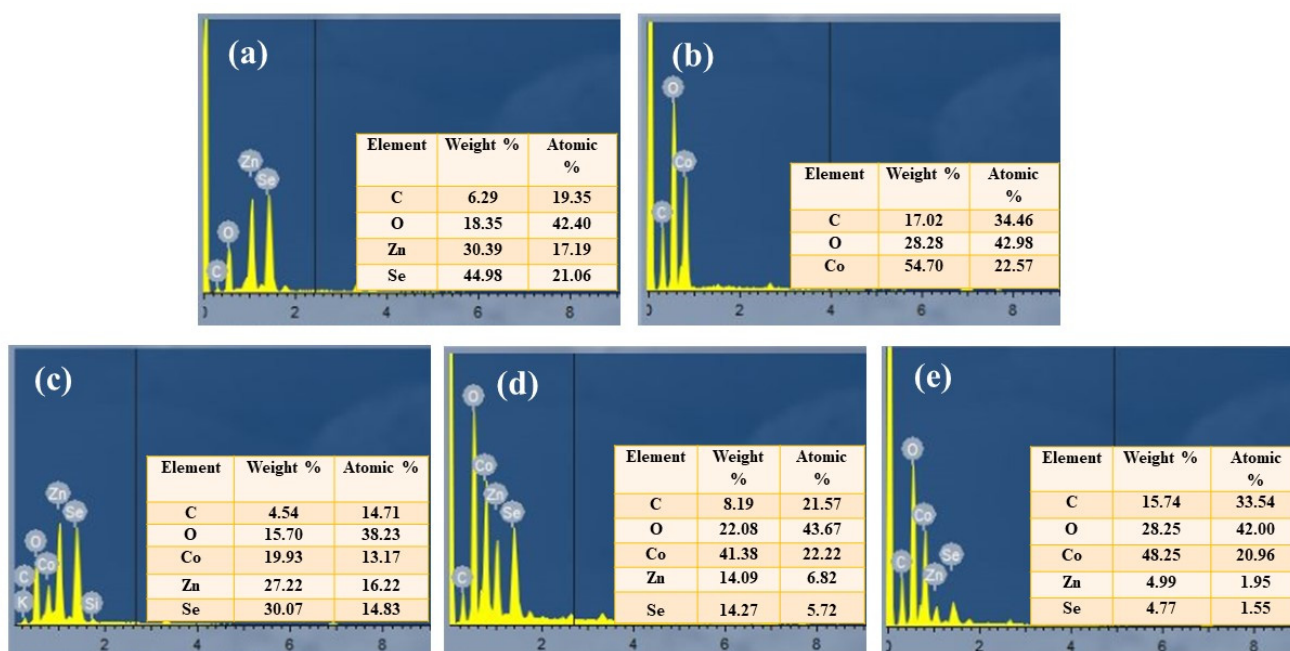


Figure 3. EDX results of (a) ZnSe, (b) Co_3O_4 , (c) Z1, (d) Z2 and (e) Z3.

The EDX results of nanocomposite ZnSe/ Co_3O_4 indicated that all the elements, i.e., Zn, Se, Co and O, are present in it, as shown in Figure 3c–e. In the nanocomposites ranging from Z1 to Z3, the composition of Zn and Se gradually decreases, which is also evident in the EDX results. In Z1, the concentration of ZnSe is higher compared to Co_3O_4 (3:1); hence, the weight and atomic percentage of Zn and Se is present in higher amounts, as shown in Figure 3c. In Z2, the concentrations of ZnSe and Co_3O_4 are equal (1:1); therefore, the weight and atomic percentage of Co and O is higher and the atomic percentage of Zn and Se is lower, compared to Z1, as shown in Figure 3d. Furthermore, in Z3, the concentration of ZnSe is lower than Co_3O_4 (1:3); therefore, the EDX exhibits a higher weight and atomic ratio for Co and O, as presented in Figure 3e.

3.4. Optical Studies and Bandgap Estimation

The optical properties and bandgap of ZnSe and Co_3O_4 have been studied with the help of the UV/visible absorption spectra and Tauc plot. During the calculations, two factors affecting the bandgap estimation were also considered: (i) the bandgap of a semiconductor nanomaterial is inversely related to the crystallite size [35], and (ii) nanomaterials with dimensions lower than the Bohr radius at an excited state absorb at higher energies [36].

ZnSe shows a sharp absorption of around 480 nm with a direct bandgap of 2.64 eV, as shown in Figure 4, which matches well with the reported value [3]. The Tauc plot is a curve in which $(\alpha h\nu)^2$ is drawn on the y-axis and $h\nu$ (eV) on the x-axis. The bandgap energy is calculated by extrapolating the graph with the help of Equation (2) [37] given below.

$$(\alpha h\nu)^n = B(h\nu - E_g) \quad (2)$$

where

$h\nu$ = photon energy (eV);

α = absorption coefficient;

B = constant relative to material;

E_g = bandgap;

$n = 1/2$ for an indirect transition and 2 for direct transition.

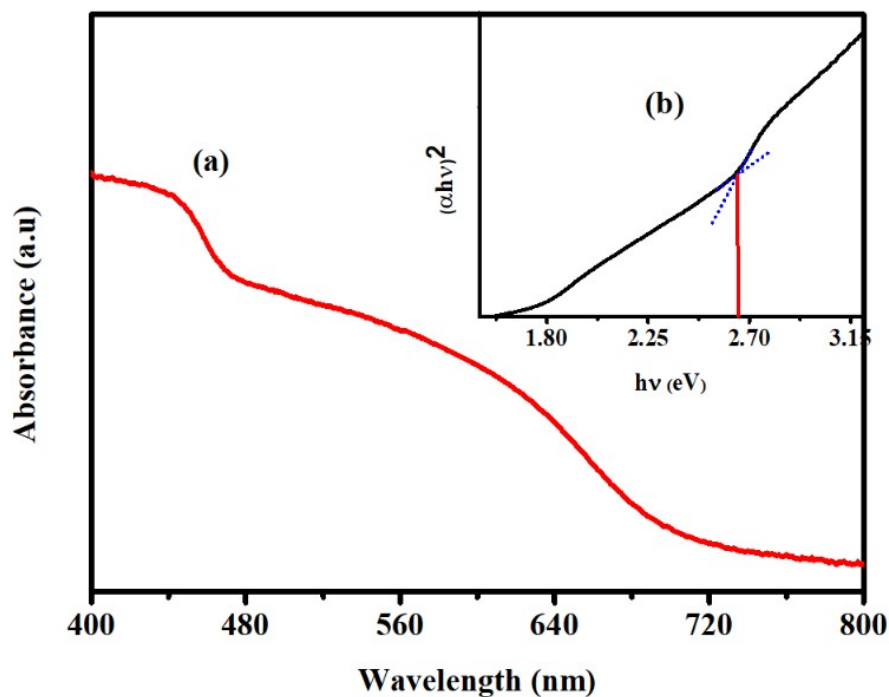


Figure 4. (a) UV/visible spectra and (b) the Tauc plot of ZnSe.

The UV/visible spectra of Co_3O_4 shows two prominent peaks, one at 510 nm and the second at 684 nm, and 2 bandgaps can be observed, ranging from 1.5 to 2.5 eV [29,38]. The calculated fundamental bandgap energy is 2.51 eV, attributed to the transfer of charge from O^{2-} to Co^{2+} , while the second bandgap energy is 2.2 eV and is attributed to the transfer of charge from O^{2-} to Co^{3+} , which is present beneath the conduction band of Co_3O_4 . The UV/visible spectra and both the bandgap energies are shown in Figure 5.

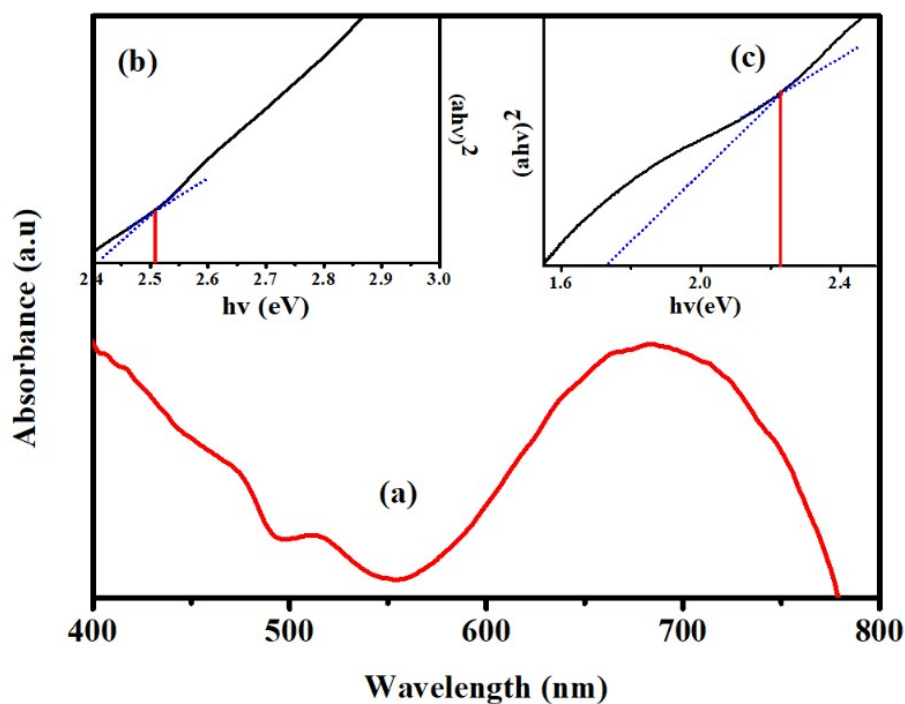


Figure 5. (a) UV/visible spectra and (b,c) the Tauc plots of Co_3O_4 . Adapted with permission from Adeel Zia et al., Journal of Materials Science: Materials in Electronics; published by Springer Nature, 2018 [29].

The valance band edge of ZnSe and Co₃O₄ are already reported in the literature. Hence, the previously reported data of XPS studies were used to calculate the conduction band position and bandgap of both the nanomaterials with the help of Equation (3).

$$E_c = E_v - E_g \quad (3)$$

where

E_c = CB energy;

E_v = VB energy;

E_g = calculated bandgap of the material.

The bandgap alignment of ZnSe/Co₃O₄ has indicated their capability as highly efficient photocatalysts under UV/visible light, as shown in Figure 6. The valence and conduction band positions of these materials were assumed from the previous reports [3,39,40].

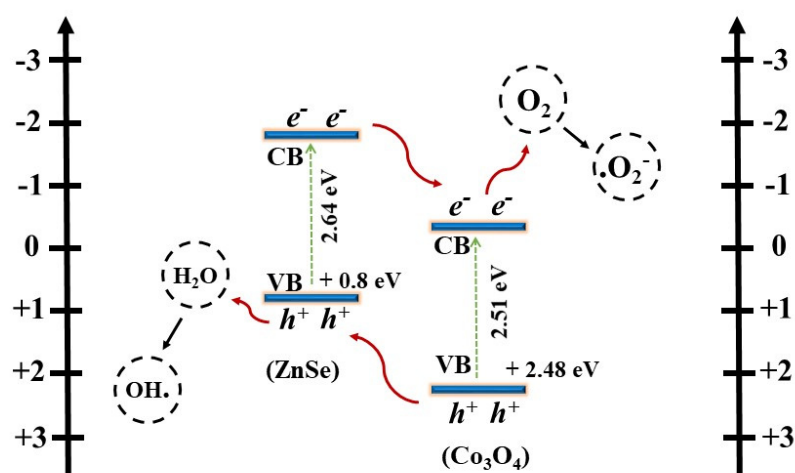


Figure 6. Schematic bandgap alignment of ZnSe/Co₃O₄.

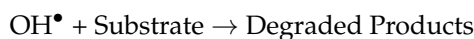
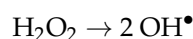
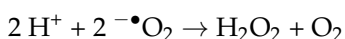
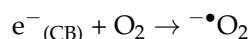
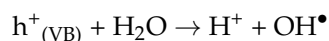
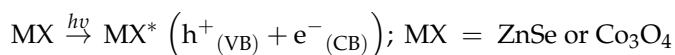
3.5. Photocatalytic Activity

Among many colored pollutants, Congo red dye is a hazardous industrial effluent ascribed to its carcinogenic properties, and extensive research was performed to degrade it via semiconductor photocatalysis. Recently, Ehsan M. F. et al. [39] reported the utilization of a g-C₃N₄/ZnSe nano-heterostructure for the photocatalytic degradation of CR dye, with a degradation efficiency of 95%. In a few other reports, ZnSe-based nanocomposites, e.g., ZnO/ZnSe [3] and ZnTe/ZnSe [31], also presented enhanced photocatalytic efficiencies of 90% and 94%, respectively. In the present work, ZnSe blends with Co₃O₄; the materials possess suitable bandgaps to prepare an excellent heterostructure for maximum charge separation as well as the surface potentials to yield reactive oxygen species, such as superoxides and hydroxide radicals. Moreover, Co₃O₄ is extensively reported as a good semiconductor photocatalyst for the degradation of organic dyes [40,41].

When UV/visible light with an intensity equal to or greater than the bandgap of the semiconductor ($h\nu \geq E_g$) is irradiated onto a photocatalyst, it excites the electrons of the semiconductor from VB to CB, leaving behind the positively charged holes in VB. These electrons and holes are the keys behind the photocatalytic reactions, but their recombination would cease the photocatalytic activity. Heterojunction formation is an excellent approach to prevent the recombination of these charges, as discussed earlier.

In the present research, the heterojunction of ZnSe and Co₃O₄ has been prepared to prohibit the electron/hole pair recombination. As shown in Figure 6, in the ZnSe/Co₃O₄ composite, the photo-excited electrons of ZnSe migrate to the CB of Co₃O₄ and the positively charged holes of Co₃O₄ migrate to the VB of ZnSe. These electron–hole pairs participate in different redox reactions, e.g., pollutant degradation and hydrogen production. Electrons present in the CB of both ZnSe and Co₃O₄ react with dissolved O to

produce $^{\bullet}\text{O}_2$ (superoxide) radical ions, which become protonated by water to produce OH^{\bullet} (hydroxyl) radicals, while the holes present in the VB of these materials produce hydroxyl radicals through the dissociation of water molecules. The hydroxyl radicals are strong oxidizing agents for pollutant degradation. Direct redox-based degradation cannot be ruled out. A generalized pathway for the formation of reactive oxygen species [39] can thus be proposed as:



After the irradiation of UV/visible light on the CR solution charged with a photocatalyst, the gradual degradation of CR dye began and continued for the next 60 min. It can be observed that the pristine nanoparticles of Co_3O_4 and ZnSe individually possess inferior photocatalytic activity than that of the nanocomposites under UV/visible light irradiation, as presented in Figure 7. Pristine Co_3O_4 possesses a low photocatalytic activity for CR dye degradation, which is about 22% in 60 min, owing to its rapid electron/hole recombination, while pristine ZnSe shows photocatalytic activity of about 64% in 60 min, which might be the result of its suitable surface potential, as indicated by Figure 6. However, ZnSe/ Co_3O_4 nanocomposites have shown a significant increase in their photocatalytic degradation efficiencies. After 60 min, the degradation efficiency of the Z1 (ZnSe/ Co_3O_4 3:1) nanocomposite reached 96%, which is the highest percentage among all the investigated nanocomposites. The reason might be the high amount of ZnSe, which has better photocatalytic activity as compared to Co_3O_4 and a better charge separation due to the optimal ratio of nanomaterials. The role of ZnSe in the overall photocatalytic degradation is high, which can be easily understood from the photocatalytic degradation efficiency of the Z3 (ZnSe/ Co_3O_4 1:3) nanocomposite showing the least degradation efficiency due to having the least amount of ZnSe. The Z2 (ZnSe/ Co_3O_4 1:1) nanocomposite shows better photocatalytic activity compared to the Z3 (ZnSe/ Co_3O_4 1:3) nanocomposite due to better charge separation. The amount of ZnSe is also greater and refers to its active catalytic role. This enhanced photodegradation activity of ZnSe/ Co_3O_4 is chiefly attributed to the reduced electron/hole recombination, due to the heterojunction formation in the nanocomposites. The bandgap alignment of ZnSe/ Co_3O_4 represents that both the charge carriers are well separated, as shown in Figure 6. Hence, the efficiency of the photocatalytic redox reaction for the degradation of Congo red dye was improved. However, the effective charge separation is not the only reason for this improved photocatalytic efficiency; there might be few other physicochemical phenomena, such as the surface charge transfer between the photocatalyst and the substrate molecule, which will be investigated in future studies.

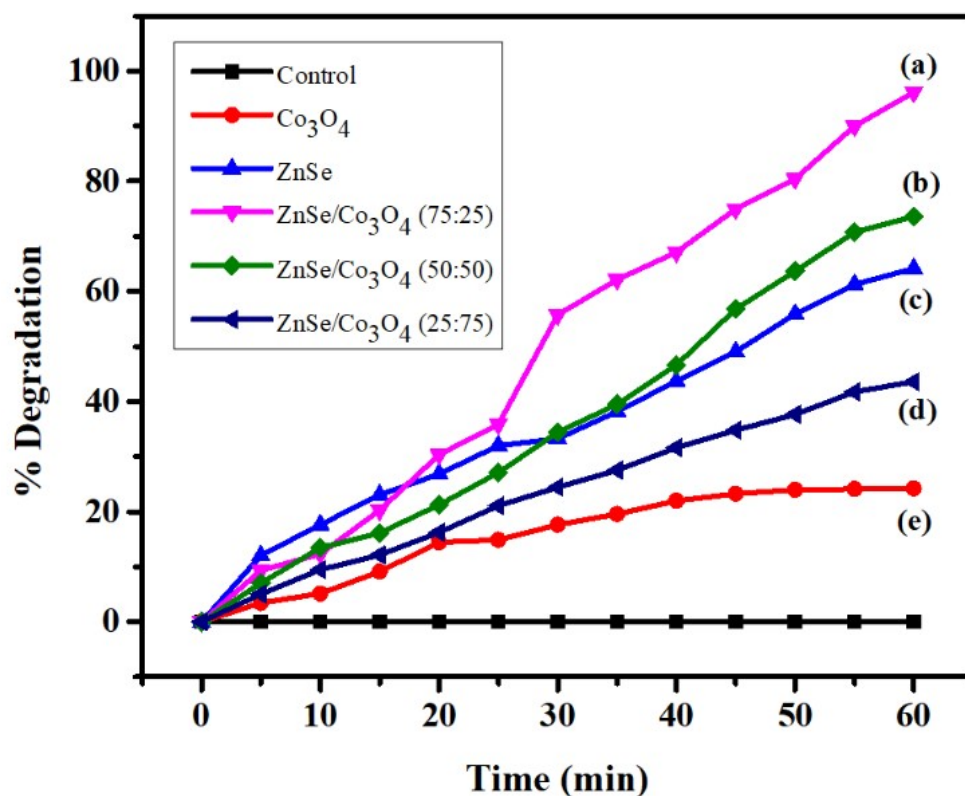


Figure 7. Photocatalytic efficiency of (a) Z1, (b) Z3, (c) ZnSe, (d) Z2 and (e) Co_3O_4 for the degradation of Congo red dye.

The photocatalytic degradation of Congo red dye is evidenced from the fall in the absorption intensity during the UV/visible analysis collected after a fixed time interval. Figure 8a represents the degradation spectra obtained during the employment of the Z1 nanocomposite, while Figure 8b indicates that negligible degradation occurs under illumination without any of the photocatalysts. A few technical articles are also being recommended, regarding the basic and detailed study surrounding visible light-driven photocatalysis [3,39,40,42,43].

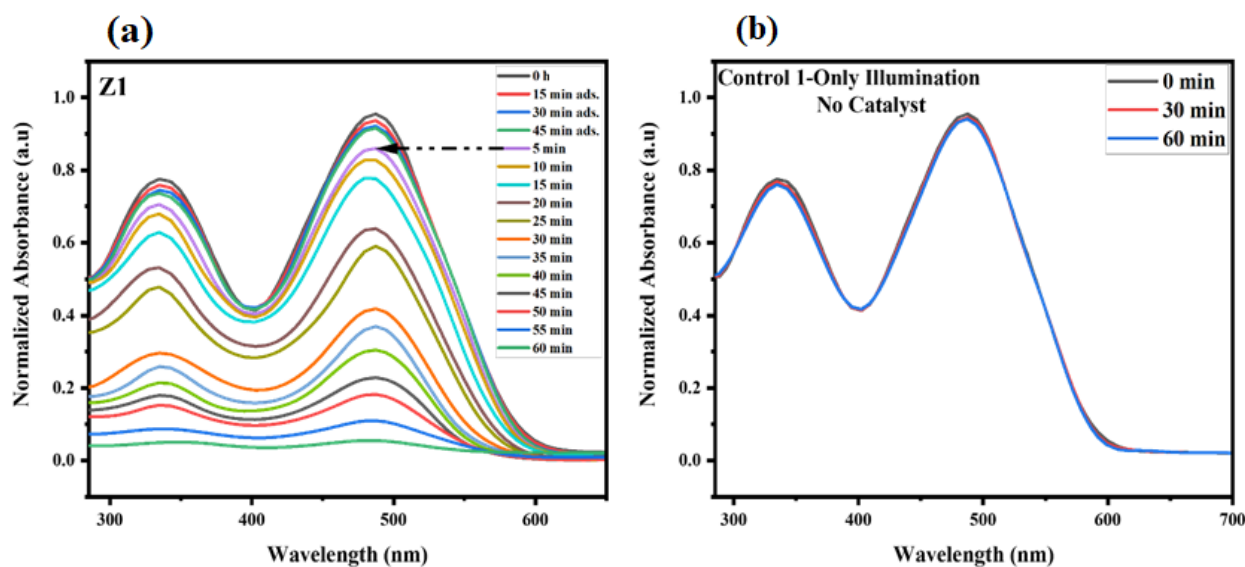


Figure 8. Degradation of Congo red dye observed for Z1 (a) and a control experiment (b).

4. Conclusions

The hydrothermal approach was applied for the preparation of ZnSe and Co₃O₄ nanoparticles, and a simple solid state method was employed for the fabrication of the ZnSe/Co₃O₄ nano-heterostructure. The prepared nanomaterials were characterized by several techniques, XRD, SEM and EDX, to investigate the crystal phase, morphology and elemental composition, respectively, while UV/visible spectroscopy was used to explore the optical properties.

The XRD pattern of ZnSe indicated the presence of both cubic and hexagonal structures, while the peaks of Co₃O₄ were in good agreement with the reported cubic structure. The intensities of both the ZnSe and Co₃O₄ characteristic peaks were varied in all the nanocomposites, in accordance with the individual component quantity, which confirmed that nanocomposites with desired compositions were successfully prepared. Scanning electron micro-images of ZnSe showed a mixed morphology, including spherical and distorted cubes or grains, while Co₃O₄ had a worm-like morphology. The EDX results showed that all the elements, Zn, Se, Co and O, are present in accordance with their anticipated amounts in the products. The UV/visible absorption spectrum of ZnSe depicted a sharp absorption of around 480 nm with a direct bandgap of 2.64 eV, while Co₃O₄ demonstrated 2 prominent peaks, 510 nm and 684 nm, corresponding to the 2 bandgaps, 2.51 eV, attributed to the transfer of charge from O²⁻ to Co²⁺ and 2.2 eV, due to the transfer of charge from O²⁻ to Co³⁺. In addition, the Tauc plot and bandgap alignment were also investigated, which confirmed that ZnSe/Co₃O₄ is a type II heterostructure. The photocatalytic activity for the degradation of Congo red dye was also analyzed and it was observed that the nano-heterostructure has exceptionally high photocatalytic efficiency. The reason might be the effective electron/hole separation due to the suitable bandgap alignment of both the nanomaterials. This study reveals the use of a nano-heterostructure for the degradation of organic pollutants, which are a major cause of environmental pollution.

Author Contributions: Conceptualization, A.Z. and M.F.E.; Methodology, A.Z.; Software, A.Z.; Validation, A.Z. and A.M.; Formal Analysis, A.Z. and A.J.; Investigation, A.Z., A.B.N. and A.J.; Resources, M.F.E.; Data Curation, A.J. and A.Z.; Writing—Original Draft Preparation, A.Z.; Writing—Review and Editing, A.M., A.J. and A.B.N.; Visualization, A.Z. and A.J.; Supervision, M.F.E.; Project Administration, A.M.; Funding Acquisition, M.F.E. All authors have read and agreed to the published version of the manuscript.

Funding: The authors are highly thankful to School of Natural Sciences at the National University of Sciences and Technology Islamabad, for providing financial support.

Data Availability Statement: Data is contained within the article.

Acknowledgments: The authors would like to acknowledge the support of the School of Chemical and Material Engineering at the National University of Sciences and Technology Islamabad Pakistan, and the Institute of Chemical Sciences at the Bahauddin Zakariya University Multan Pakistan, for providing support for the characterization of the prepared samples.

Conflicts of Interest: The authors declare no conflict of interest.

References

1. Rochkind, M.; Pasternak, S.; Paz, Y. Using Dyes for Evaluating Photocatalytic Properties: A Critical Review. *Molecules* **2015**, *20*, 88–110. [[CrossRef](#)] [[PubMed](#)]
2. Sakthivel, S.; Neppolian, B.; Shankar, M.V.; Arabindoo, B.; Palanichamy, M.; Murugesan, V. Solar Photocatalytic Degradation of Azo Dye: Comparison of Photocatalytic Efficiency of ZnO and TiO₂. *Sol. Energy Mater. Sol. Cells* **2003**, *77*, 65–82. [[CrossRef](#)]
3. Ehsan, M.F.; Bashir, S.; Hamid, S.; Zia, A.; Abbas, Y.; Umbreen, K.; Ashiq, M.N.; Shah, A. One-Pot Facile Synthesis of the ZnO/ZnSe Heterostructures for Efficient Photocatalytic Degradation of Azo Dye. *Appl. Surf. Sci.* **2018**, *459*, 194–200. [[CrossRef](#)]
4. Prasannan, A.; Udomsin, J.; Tsai, H.-C.; Wang, C.-F.; Lai, J.-Y. Robust Underwater Superoleophobic Membranes with Bio-Inspired Carrageenan/Laponite Multilayers for the Effective Removal of Emulsions, Metal Ions, and Organic Dyes from Wastewater. *Chem. Eng. J.* **2020**, *391*, 123585. [[CrossRef](#)]
5. Rashidi, H.R.; Sulaiman, N.M.N.; Hashim, N.A.; Hassan, C.R.C.; Ramli, M.R. Synthetic Reactive Dye Wastewater Treatment by Using Nano-Membrane Filtration. *Desalination Water Treat.* **2015**, *55*, 86–95. [[CrossRef](#)]

6. Tung, C.-H.; Shen, S.-Y.; Chang, J.-H.; Hsu, Y.-M.; Lai, Y.-C. Treatment of Real Printing Wastewater with an Electrocatalytic Process. *Sep. Purif. Technol.* **2013**, *117*, 131–136. [[CrossRef](#)]
7. Electrocatalytic Degradation of Bromocresol Green Wastewater on Ti/SnO₂-RuO₂ Electrode | Water Science and Technology | IWA Publishing. Available online: <https://iwaponline.com/wst/article-abstract/75/1/220/19781> (accessed on 4 December 2020).
8. Charentanyarak, L. Heavy Metals Removal by Chemical Coagulation and Precipitation. *Water Sci. Technol.* **1999**, *39*, 135–138. [[CrossRef](#)]
9. Ali, I.; Gupta, V.K. Advances in Water Treatment by Adsorption Technology. *Nat. Protoc.* **2006**, *1*, 2661. [[CrossRef](#)] [[PubMed](#)]
10. Bhatia, D.; Sharma, N.R.; Singh, J.; Kanwar, R.S. Biological Methods for Textile Dye Removal from Wastewater: A Review. *Crit. Rev. Environ. Sci. Technol.* **2017**, *47*, 1836–1876.
11. Sonkusare, V.N.; Chaudhary, R.G.; Bhusari, G.S.; Mondal, A.; Potbhare, A.K.; Mishra, R.K.; Juneja, H.D.; Abdala, A.A. Mesoporous Octahedron-Shaped Tricobalt Tetroxide Nanoparticles for Photocatalytic Degradation of Toxic Dyes. *ACS Omega* **2020**, *5*, 7823–7835. [[CrossRef](#)] [[PubMed](#)]
12. Lam, S.-M.; Sin, J.-C.; Abdullah, A.Z.; Mohamed, A.R. Degradation of Wastewaters Containing Organic Dyes Photocatalysed by Zinc Oxide: A Review. *Desalination Water Treat.* **2012**, *41*, 131–169. [[CrossRef](#)]
13. Shanker, U.; Jassal, V.; Rani, M. Catalytic Removal of Organic Colorants from Water Using Some Transition Metal Oxide Nanoparticles Synthesized under Sunlight. *RSC Adv.* **2016**, *6*, 94989–94999. [[CrossRef](#)]
14. Kiwaan, H.A.; Atwee, T.M.; Azab, E.A.; El-Bindary, A.A. Photocatalytic Degradation of Organic Dyes in the Presence of Nanostructured Titanium Dioxide. *J. Mol. Struct.* **2020**, *1200*, 127115. [[CrossRef](#)]
15. Al-Mamun, M.R.; Kader, S.; Islam, M.S.; Khan, M.Z.H. Photocatalytic Activity Improvement and Application of UV-TiO₂ Photocatalysis in Textile Wastewater Treatment: A Review. *J. Environ. Chem. Eng.* **2019**, *7*, 103248.
16. Effect of Various Amounts of Graphene Oxide on the Degradation Characteristics of the ZnSe/Graphene Nanocomposites. *Appl. Surf. Sci.* **2015**, *358*, 63–69. [[CrossRef](#)]
17. Raza, N.; Raza, W.; Gul, H.; Kim, K.-H. ZnO-ZnTe Hierarchical Superstructures as Solar-Light-Activated Photocatalysts for Azo Dye Removal. *Environ. Res.* **2020**, *194*, 110499. [[CrossRef](#)] [[PubMed](#)]
18. Shawky, A.; El-Sheikh, S.M.; Gaber, A.; El-Hout, S.I.; El-Sherbiny, I.M.; Ahmed, A.I. Urchin-like CuS Nanostructures: Simple Synthesis and Structural Optimization with Enhanced Photocatalytic Activity under Direct Sunlight. *Appl. Nanosci.* **2020**, *10*, 2153–2164. [[CrossRef](#)]
19. Korala, L.; Germain, J.R.; Chen, E.; Pala, I.R.; Li, D.; Brock, S.L. CdS Aerogels as Efficient Photocatalysts for Degradation of Organic Dyes under Visible Light Irradiation. *Inorg. Chem. Front.* **2017**, *4*, 1451–1457. [[CrossRef](#)] [[PubMed](#)]
20. Aziz, A.; Ali, N.; Khan, A.; Bilal, M.; Malik, S.; Ali, N.; Khan, H. Chitosan-zinc Sulfide Nanoparticles, Characterization and Their Photocatalytic Degradation Efficiency for Azo Dyes. *Int. J. Biol. Macromol.* **2020**, *153*, 502–512. [[CrossRef](#)]
21. Ayodhya, D.; Veerabhadram, G. A Review on Recent Advances in Photodegradation of Dyes Using Doped and Heterojunction Based Semiconductor Metal Sulfide Nanostructures for Environmental Protection. *Mater. Today Energy* **2018**, *9*, 83–113. [[CrossRef](#)]
22. Dong, H.; Li, J.; Chen, M.; Wang, H.; Jiang, X.; Xiao, Y.; Tian, B.; Zhang, X. High-Throughput Production of ZnO-MoS₂-Graphene Heterostructures for Highly Efficient Photocatalytic Hydrogen Evolution. *Materials* **2019**, *12*, 2233. [[CrossRef](#)]
23. Ritika; Kaur, M.; Umar, A.; Mehta, S.K.; Singh, S.; Kansal, S.K.; Fouad, H.; Allothman, O.Y. Rapid Solar-Light Driven Superior Photocatalytic Degradation of Methylene Blue Using MoS₂-ZnO Heterostructure Nanorods Photocatalyst. *Materials* **2018**, *11*, 2254. [[CrossRef](#)] [[PubMed](#)]
24. Shanmugaratnam, S.; Velauthapillai, D.; Ravirajan, P.; Christy, A.A.; Shivatharsiny, Y. CoS₂/TiO₂ Nanocomposites for Hydrogen Production under UV Irradiation. *Materials* **2019**, *12*, 3882. [[CrossRef](#)] [[PubMed](#)]
25. Ahmad, I. Comparative Study of Metal (Al, Mg, Ni, Cu and Ag) Doped ZnO/g-C₃N₄ Composites: Efficient Photocatalysts for the Degradation of Organic Pollutants. *Sep. Purif. Technol.* **2020**, *251*, 117372. [[CrossRef](#)]
26. Mohammed, R.; Ali, M.E.M.; Gomaa, E.; Mohsen, M. Green ZnO Nanorod Material for Dye Degradation and Detoxification of Pharmaceutical Wastes in Water. *J. Environ. Chem. Eng.* **2020**, *8*, 104295. [[CrossRef](#)]
27. Choudhary, S.; Sahu, K.; Bisht, A.; Satpati, B.; Mohapatra, S. Rapid Synthesis of ZnO Nanowires and Nanoplates with Highly Enhanced Photocatalytic Performance. *Appl. Surf. Sci.* **2020**, *541*, 148484. [[CrossRef](#)]
28. Rani, E.G.D.S.; Kumar, G.A.; Steplinpaulselvin, S.; Rajaram, R.; Silambarasan, T.S.; Lydia, S.L.; Chen, Y. Survival Assessment of Simple Food Webs for Dye Wastewater after Photocatalytic Degradation Using SnO₂/GO Nanocomposites under Sunlight Irradiation. *Sci. Total Environ.* **2020**, *721*, 137805. [[CrossRef](#)]
29. Zia, A.; Hamid, S.; Ehsan, M.F.; Allah, S.U.; Ashiq, M.N.; Shah, A. Congo Red Photomineralization over Co₃O₄/CoTe Common Cation Nanocomposites. *J. Mater. Sci. Mater. Electron.* **2018**, *29*, 20271–20279. [[CrossRef](#)]
30. Sharma, M.; Poddar, M.; Gupta, Y.; Nigam, S.; Avasthi, D.K.; Adeling, R.; Abolhassani, R.; Fiutowski, J.; Joshi, M.; Mishra, Y.K. Solar Light Assisted Degradation of Dyes and Adsorption of Heavy Metal Ions from Water by CuO-ZnO Tetrapodal Hybrid Nanocomposite. *Mater. Today Chem.* **2020**, *17*, 100336. [[CrossRef](#)]
31. Ehsan, M.F.; Qudoos, S.; Ahmad, Z.; Hamid, S.; Arfan, M.; Zia, A.; Umbreen, K.; Ashiq, M.N.; Tyagi, D. ZnTe/ZnSe Heterostructures: In-Situ Synthesis, Characterization and Photocatalytic Activity for Congo Red Degradation. *SN Appl. Sci.* **2019**, *1*, 197. [[CrossRef](#)]
32. Chen, Y.; Qian, J.; Wang, N.; Xing, J.; Liu, L. In-Situ Synthesis of CNT/TiO₂ Heterojunction Nanocomposite and Its Efficient Photocatalytic Degradation of Rhodamine B Dye. *Inorg. Chem. Commun.* **2020**, *119*, 108071. [[CrossRef](#)]

33. Kim, M.-J.; Choi, Y.I.; Joo, S.W.; Kang, M.; Sohn, Y. Synthesis of Er and Yb-Doped Cubic and Hexagonal Phase ZnSe Nano-Assembled Microspheres and Their Photocatalytic Activities. *Ceram. Int.* **2014**, *40*, 16051–16059. [[CrossRef](#)]
34. Xue, X.-Y.; Yuan, S.; Xing, L.-L.; Chen, Z.-H.; He, B.; Chen, Y.-J. Porous Co₃O₄ Nanoneedle Arrays Growing Directly on Copper Foils and Their Ultrafast Charging/Discharging as Lithium-Ion Battery Anodes. *Chem. Commun.* **2011**, *47*, 4718–4720. [[CrossRef](#)]
35. Wang, G.; Shen, X.; Horvat, J.; Wang, B.; Liu, H.; Wexler, D.; Yao, J. Hydrothermal Synthesis and Optical, Magnetic, and Supercapacitance Properties of Nanoporous Cobalt Oxide Nanorods. *J. Phys. Chem. C* **2009**, *113*, 4357–4361. [[CrossRef](#)]
36. Gu, F.; Wang, S.F.; Lü, M.K.; Zhou, G.J.; Xu, D.; Yuan, D.R. Photoluminescence Properties of SnO₂ Nanoparticles Synthesized by Sol-Gel Method. *J. Phys. Chem. B* **2004**, *108*, 8119–8123. [[CrossRef](#)]
37. Kim, K.J.; Park, Y.R. Optical Investigation of Charge-Transfer Transitions in Spinel Co₃O₄. *Solid State Commun.* **2003**, *127*, 25–28. [[CrossRef](#)]
38. Barakat, N.A.; Khil, M.S.; Sheikh, F.A.; Kim, H.Y. Synthesis and Optical Properties of Two Cobalt Oxides (CoO and Co₃O₄) Nanofibers Produced by Electrospinning Process. *J. Phys. Chem. C* **2008**, *112*, 12225–12233. [[CrossRef](#)]
39. Ehsan, M.F.; Shafiq, M.; Hamid, S.; Shafiee, A.; Usman, M.; Khan, I.; Ashiq, M.N.; Arfan, M. Reactive Oxygen Species: New Insights into Photocatalytic Pollutant Degradation over g-C₃N₄/ZnSe Nanocomposite. *Appl. Surf. Sci.* **2020**, *532*, 147418.
40. Xiao, Q.; Zhang, J.; Xiao, C.; Tan, X. Photocatalytic Degradation of Methylene Blue over Co₃O₄/Bi₂WO₆ Composite under Visible Light Irradiation. *Catal. Commun.* **2008**, *9*, 1247–1253. [[CrossRef](#)]
41. Han, C.; Ge, L.; Chen, C.; Li, Y.; Xiao, X.; Zhang, Y.; Guo, L. Novel Visible Light Induced Co₃O₄-g-C₃N₄ Heterojunction Photocatalysts for Efficient Degradation of Methyl Orange. *Appl. Catal. B Environ.* **2014**, *147*, 546–553. [[CrossRef](#)]
42. Gholami, P.; Khataee, A.; Bhatnagar, A.; Vahid, B. Synthesis of N-Doped Magnetic WO_{3-x}@ Mesoporous Carbon Using a Diatom Template and Plasma Modification: Visible-Light-Driven Photocatalytic Activities. *ACS Appl. Mater. Interfaces* **2021**, *13*, 13072–13086. [[CrossRef](#)] [[PubMed](#)]
43. Moradi, M.; Vasseghian, Y.; Khataee, A.; Harati, M.; Arfaeinia, H. Ultrasound-assisted synthesis of FeTiO₃/GO nanocomposite for photocatalytic degradation of phenol under visible light irradiation. *Sep. Purif. Technol.* **2021**, *261*, 118274. [[CrossRef](#)]